Author/s:
Yuan, G;Ritchie, C;Ritter, M;Murphy, S;Gómez, DE;Mulvaney, P

Title:
The Degradation and Blinking of Single CsPbI3 Perovskite Quantum Dots

Date:
2018-06-28

Citation:
Yuan, G., Ritchie, C., Ritter, M., Murphy, S., Gómez, D. E. & Mulvaney, P. (2018). The Degradation and Blinking of Single CsPbI3 Perovskite Quantum Dots. Journal of Physical Chemistry C, 122 (25), pp.13407-13415. https://doi.org/10.1021/acs.jpcc.7b11168.

Persistent Link:
https://hdl.handle.net/11343/344945

The Degradation and Blinking of Single $CsPbI_3$ Perovskite Quantum Dots

Gangcheng Yuan,† Cameron Ritchie,† Maria Ritter,† Sean Murphy,† Daniel E. Gómez, ‡ and Paul Mulvaney†*

†ARC Centre of Excellence in Exciton Science, School of Chemistry,

University of Melbourne, Parkville, Victoria 3010, Australia

‡RMIT University, Melbourne, Victoria, 3000, Australia

AUTHOR INFORMATION

Corresponding Author

*E-mail: mulvaney@unimelb.edu.au

ABSTRACT: We demonstrate using single molecule spectroscopy that inorganic $CsPbI_3$ perovskite quantum dots (PQDs) undergo an irreversible, photo-accelerated reaction with water that results in a blueshift of its photoluminescence (PL) and ultimately to complete quenching of the emission. We find that decomposition does not take place in the presence of oxygen alone, but that it requires light and water. We also analyze the blinking

for some stable PQDs and find a continuous distribution of emission states with a linear correlation between intensity and lifetime. We postulate that, in addition to charging and discharging processes, blinking arises from the activation and deactivation of non-radiative recombination centers in the PQDs.

INTRODUCTION

The efficiency of perovskite based solar cells has improved from 3.8% to more than 20% within just a few years[1-5], and as a result, organometallic perovskites have become one of the most studied optoelectronic materials. Recently, all-inorganic lead halide perovskite colloidal nanocrystals (NCs) have been successfully synthesized with high luminescence quantum yields (QYs) and tunable emission spectra covering the entire visible spectral range[6-9]. Like the organic-inorganic lead halide perovskites (hybrid lead halide perovskites), the all-inorganic perovskites have potential uses in light-emitting diodes,[10-13] solar cells,[14-15] and tunable lasers.[16-18] Compared to the low PL QY of bare CdSe QDs, the PL QY of as-synthesized $CsPbX_3$ is up to 90%, even without any additional surface passivation. However, all-inorganic lead halide perovskites still suffer from the same stability problems as hybrid lead halide perovskites. The instability not only limits the performance of perovskite devices but may also result in the release of toxic Pb (II) ions from these devices as a consequence of decomposition. The degradation of perovskite materials has been attributed to many factors such as moisture,[19-22] thermal effects,[23-24] oxygen,[25] and light exposure.[26-29] It has been reported that an inorganic–organic hybrid ion pair[30] or cross-linking of certain ligands by X-ray

irradiation[31] can produce stable all-inorganic perovskite films under a humid environment and high pump power excitation. However, more commonly, chemical degradation of perovskite materials can be partially solved through encapsulation.[6, 32-33] Although more stable than their organo-metal counterparts, there has been little work on the underpinning chemistry that leads to degradation of inorganic perovskites. To glean information on the degradation process it is useful to study single perovskite nanocrystals. Spectroscopy studies allow the roles of trions, surface traps and biexcitons during charge carrier relaxation in semiconductor nanocrystals to be elucidated.

The biexciton lifetime in single PQDs is much shorter than that in CdSe nanocrystals of a similar size,[34-36] due to faster Auger recombination in PQDs. This also leads to strong photon antibunching, which makes single $CsPbX_3$ PQDs potential single-photon sources.[37-39] At low temperature, single $CsPbX_3$ PQDs exhibit stable and narrow-band emission with suppressed blinking.[40] Varying the anion composition is a possible way to control blinking, and may enable synthesis of non-blinking PQDs.[41] However, blinking is still a serious problem in PQDs. Blinking in $CsPbX_3$ PQDs has been attributed to a process of charging and discharging.[37] Although an emissive charged state is possible in non-blinking PQDs,[42] in general, the picosecond nonradiative Auger recombination overwhelms the nanosecond-scale radiative recombination, leading to weak emission from the charged exciton.[37]

Here we have used a confocal microscope to track the fluorescence evolution of single $CsPbI_3$ PQDs under various environmental conditions including: air, dry nitrogen, wet nitrogen, dry oxygen, and wet oxygen. We show that fast decomposition of $CsPbI_3$ takes place under illumination in a moist atmosphere. We also examine the mechanism of blinking for the stable PQDs. In addition to *on* and *off* states, a set of continuous emission states arises due to the activation and deactivation of non-radiative recombination centers. This suggests that surface states may be efficient recombination sites and that passivation strategies to remove surface defects will lead to strong improvements in photostability.

METHODS

Synthesis of Colloidal $CsPbI_3$ and $CsPbBr_3$ QDs. To prepare cesium oleate, Cs_2CO_3 (0.2 g), octadecene (7.5 ml) and oleic acid (0.625 ml) were mixed and then heated to 150 °C until the solution was clear. Cs-oleate was then cooled and kept at 100 °C before injection. For PQD synthesis, first octadecene (5 ml) and PbI_2 (0.084 g) ($PbBr_2$ (0.069 g)) were loaded into a three-neck flask, and then heated to 120 °C for 1 hour. After injecting oleic acid (0.5 ml) and oleylamine (0.5 ml), the mixture was heated to 150 °C again. As soon as the temperature reached to 150 °C, cesium oleate (0.4 ml) was quickly injected and the flask cooled rapidly. All preparation and reactions were completed in a nitrogen glovebox without contacting water and oxygen. The PQDs were precipitated by centrifugation, redispersed in hexane, and stored in the glovebox.

Characterization The absorption spectra and the fluorescence spectra were collected with an Agilent 8453 UV-visible Spectroscopy System and a Fluorolog Spectrofluorometer (HORIBA Scientific), respectively. The PL QYs of the PQDs were calculated by Rhodamine 101 as a reference and taking its luminescence QY to be 0.96.

Confocal scanning PL images and single QD spectroscopy Small drops of dilute PQD hexane solution were cast on coverslips. Single PQDs or clusters were distributed sparsely after spincoating. Then the coverslips were loaded into a sealed chamber. All sample preparation was carried out in a nitrogen glovebox before the chamber was taken out for measurement. A 466 nm pulsed laser diode (PicoQuant, LDH-P-C-470) was used to excite PQDs via a confocal microscope (Olympus IX 71) with an oil-immersion objective (Olympus, PlanApo NA 1.4). The excitation power was 100 nW, corresponding to a low excitation rate of 0.045. The collected emission was split into two parts. For scanning PL image, PL decay, and PL trajectory, one part of the emission was sent to avalanche photodiodes (APDs, Perkin-Elmer, SPCM-AQR-14) connected to a time-correlated single photon counting (TCSPC) card; for spectra, the other part of the emission was sent to a TRIAX 550 spectrometer equipped with a liquid nitrogen cooled Symphony 3000 CCD (HORIBA Scientific). During the measurements, the gas in the chamber was changed by flushing with each new gas for 10 minutes. Wet oxygen and nitrogen were produced by water bubbling. In order to obtain pure wet nitrogen, the water was pretreated by bubbling with nitrogen for one hour to remove the dissolved oxygen.

RESULTS AND DISCUSSION

The $CsPbI_3$ perovskite quantum dots were synthesized following a previous report[6] (see experiment details in Supporting Information). According to TEM (Figure 1a), the quantum dot size is 10.9 ± 1.1 nm, which is below the effective Bohr diameter of 12 nm.[6] Figure 1b shows the PL and absorption spectra. The PL spectral peak is located at 674 nm, the full width at half-maximum (FWHM) is 33 nm, and the quantum yield is estimated to be 78%. Since there is no significant change in PL intensity or spectral peak in Figure 1c, the $CsPbI_3$ PQDs are considered stable in hexane stored in the dark under air for at least one month. Although there is no obvious PL spectral shift, fast degradation is observed for a PQD film in air (Figure 1d). Before the fast decrease, however, the PL intensity increases for the first 120 minutes. This PL enhancement (photo-brightening) is possibly due to photo-activation[43-45] before photo-degradation. Photo-brightening is a general phenomenon in metal chalcogenide QDs, which is attributed to many factors including the passivation of surface traps.[46-49]

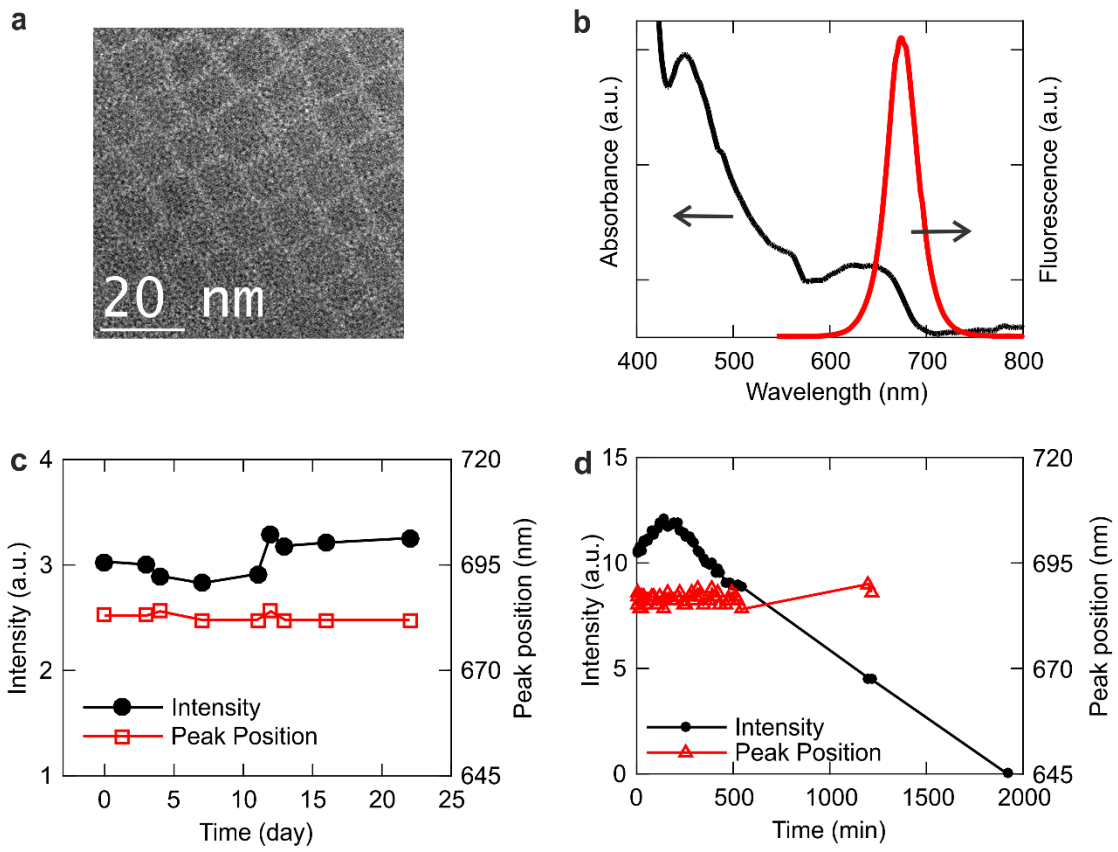

Figure 1 (a) A representative TEM of $CsPbI_3$ PQDs. The QD size is 10.9 ± 1.1 nm. (b) Absorption and emission spectra of ensemble $CsPbI_3$ PQDs in hexane. The emission spectral peak wavelength is 674 nm, and the QY is 78%. (c) PL intensity and spectral peak position of $CsPbI_3$ PQDs in hexane stored in the dark under air. (d) PL intensity and spectral peak position of a $CsPbI_3$ PQD film on glass in air.

Moisture and oxygen may contribute to the photo-brightening process. Moisture-induced degradation is a notorious problem but a certain amount of exposure to moisture is not always bad, for it can also reduce the trap density in methylammonium lead halide perovskite films and improve the performance of solar cells.[21] The function of oxygen in PL is also controversial: oxygen can cause photo-brightening,[45] but it can also act as a scavenger of

photoexcited electrons and quench the fluorescence.[50] Further experiments are needed to clarify the mechanism of the photo-brightening and photo-darkening.

To obtain information on the degradation process at the single-QD level, we have measured the PL from single PQDs in dry nitrogen or ambient air with a confocal microscope. Confocal scanning PL images were recorded sequentially for the same 10 μm×10 μm areas. The white spots in the images are due to the PL from single PQDs or clusters. Each image scan took 15 min, so the same single quantum dot can be tracked every 15 min using continuous scanning cycles. While some PQDs flicker or photo-brighten in the sealed chamber filled with dry nitrogen, there is no degradation over a 90 minute period (Figure 2a). In fact, single $CsPbI_3$ PQDs are still bright even after one day when left in a nitrogen chamber. However, once exposed to air (the lab ambient humidity was 60 ± 5% during the experiments), both the size and number of bright spots decrease (Figure 2b). Finally, all PQDs are non-luminescent within one hour. The large, bright spots in Figure 2b correspond to large clusters of PQDs. As surface to volume ratio is smaller for PQD clusters, these bright spots disappear more slowly than the smaller spots due to PL from single PQDs.

Although the laser can drive or promote degradation (as we show later), it is not responsible for the fast degradation observed here for two reasons: firstly, the laser spot only stays on the same PQDs for a very short time during each scan (the line scanning speed is 0.1μm/s); secondly, after exposure to ambient air for one hour, no fluorescence can be

detected from the regions which remained in the dark (*e.g.*, no prior laser illumination). Thus, it is a dark process in ambient air that causes the fast degradation of $CsPbI_3$ PQDs.

The fast degradation of $CsPbI_3$ PQDs is in sharp contrast to that of $CsPbBr_3$ PQDs. Some $CsPbBr_3$ PQDs remain bright even after leaving in ambient air for several hours (Figures S2-3 in Supporting Information). It is also reported that cubic $CsPbI_3$ NCs recrystallizes into a yellow orthorhombic phase after long-time storage (months) while other $CsPbX_3$ (Br or Cl) NCs remain stable.[6]

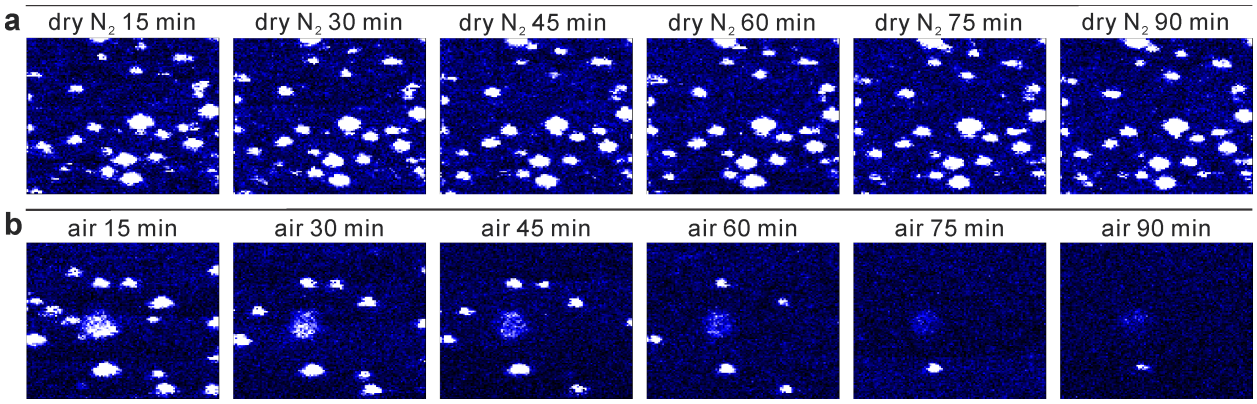

Figure 2 Continuous confocal scanning PL images of $CsPbI_3$ PQDs (10 μm×10 μm). The scanning time of each image is 15 min. The bright spots represent single PQDs or clusters. Images in (a) were recorded sequentially for a region in dry nitrogen. Images in (b) were recorded sequentially for another region of the same sample in air. The relative humidity in air was 60 ± 5%.

It is postulated that moisture in air can induce the degradation of perovskites. To confirm this, we monitored the fluorescence change under controlled atmospheric conditions (dry nitrogen, wet nitrogen, dry oxygen, and wet oxygen) for single $CsPbI_3$ PQDs, as shown in Figure 3. Initially, single PQDs are placed in a sealed chamber filled with dry nitrogen; when dry oxygen (Figure 3a) or dry nitrogen (Figure 3c) flows into the chamber, there is no change in fluorescence intensity, for at least 90 min. Hence, oxygen alone does not cause the degradation of $CsPbI_3$ over short periods. When wet oxygen (Figure 3b) or wet nitrogen (Figure 3d) enters and the relative humidity exceeds 80%, the degradation is substantially faster than in ambient air, which has a relative humidity of approximately 60%. Therefore, we conclude it is not oxygen but moisture alone that is responsible for the fast degradation of $CsPbI_3$ QDs in the dark.

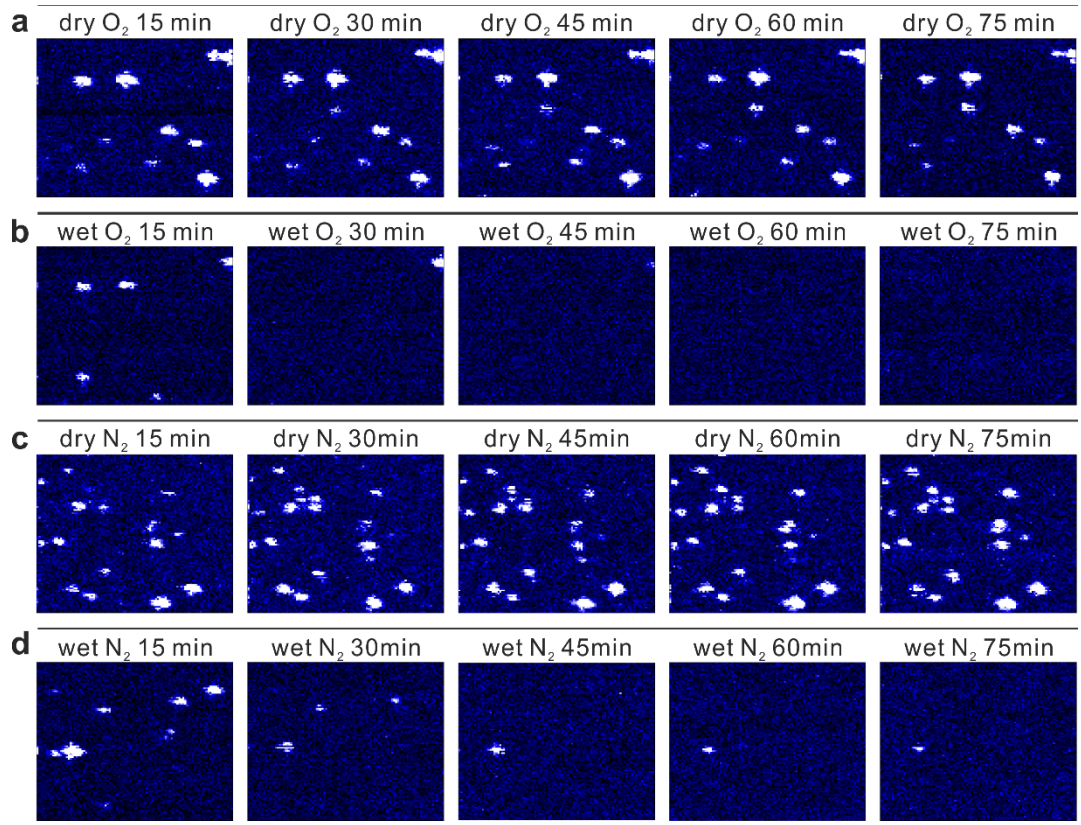

Figure 3 Continuous confocal scanning PL images of $CsPbI_3$ PQDs (10 μm×10 μm). The scanning time of each image is 15 min. The bright spots represent single PQDs or clusters. Images in (a) and (b) were recorded sequentially for a region in dry and wet oxygen, respectively. Images in (c) and (d) were recorded sequentially for a region of a new sample in dry and wet nitrogen, respectively.

In order to investigate the effect of light on the degradation, we measured the change in the fluorescence intensity for single $CsPbI_3$ PQDs under continuous excitation in dry nitrogen, dry oxygen, and ambient air. We define the photostability lifetime of PQDs under laser illumination as the time it takes for the emission intensity to decrease to half of its initial value. The average photostability lifetime was found to be 47 ± 29 s for 9 $CsPbI_3$ PQDs

in ambient air, 288 ± 195 s for 18 $CsPbI_3$ PQDs in dry nitrogen, and 267 ± 108s for 15 $CsPbI_3$ PQDs in dry oxygen with an excitation power of 100 nW at 466 nm. Under nitrogen, continuous laser exposure switches off the PQDs completely in 5-10 min, while in the dark there is no change for more than 90 min as we have shown in Figure 2a. This illustrates that light accelerates the degradation process.

Time-dependent PL spectra were also collected for $CsPbI_3$ PQDs. According to the results presented for three representative single $CsPbI_3$ PQDs in Figures 4a-c, no matter what the environment, there is always a blueshift in the PL spectra and a steady decrease in intensity during illumination. It has been reported that photo-oxidation occurs in methylammonium lead trihalides in the presence of oxygen.[25] For $CsPbI_3$ PQDs, however, there is no obvious difference between the degradation rates in dry nitrogen and dry oxygen, likely due to the fact that $CsPbI_3$ PQDs contains no organic moiety that can be oxidized. Under continuous excitation in humid air, the fluorescence lasts for less than 2 min for most of these PQDs. Furthermore, the fluorescence peak blueshifts faster in humid air compared to the rate in a dry environment.

In Figure 4d, the light induced spectral peak shifts (from 670 nm to 590 nm) are presented as a function of time. The blueshift indicates that the effective size of the quantum dots decreases due to decomposition. Using the effective mass approximation (EMA), we find that the blueshift corresponds to a constant rate of decrease in diameter as shown in Figure 4e (see the calculation in Supporting Information). For all-inorganic PQDs, we infer that the degradation occurs *via* a simple process assisted by water or light:[19, 25]

$$CsPbI_3 \xrightarrow{H_2O,light} CsI(aq) + PbI_2$$

In this process, $CsPbI_3$ PQDs decompose layer by layer (starting from the outside layer) at a constant rate, resulting in a constant rate of size decrease and blueshift. The statistics of the blue-shift rates for additional PQDs are given in Figure 4f.

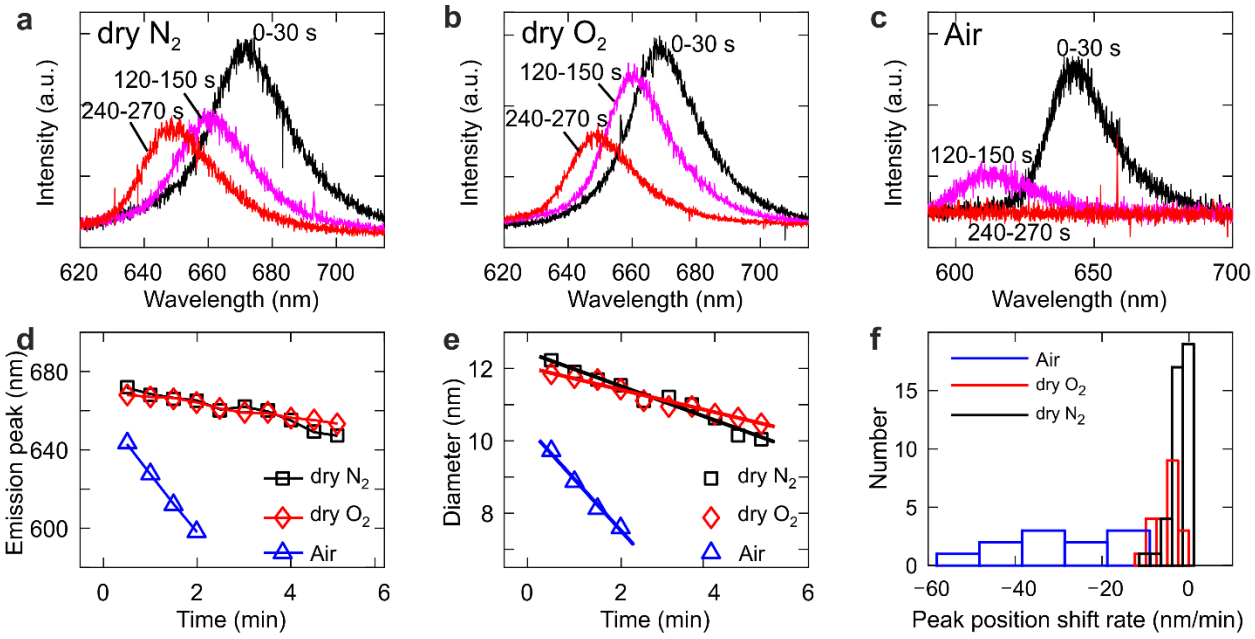

Figure 4 The PL spectral shifts of single $CsPbI_3$ PQDs as a function of time with a laser illumination. The integration time of each spectrum is 30 seconds. The excitation wavelength is 466 nm, and the power is 100 nW. There is a trend of intensity decrease and blueshift in (a) dry nitrogen, (b) dry oxygen, and (c) air. (d) Emission spectral peak position of PQDs in dry nitrogen (black squares), dry oxygen (red diamonds), and air (blue triangles). The lines are guides for the eye. (e) Calculated size of the PQDs as a function of time based on the effective mass approximation. The rates at which the size decreases are: 0.13 nm/min in dry

nitrogen (black squares), 0.09 nm/min in dry oxygen (red diamonds), and 0.62 nm/min in air (blue triangles). (f) Statistics for the blue-shift rates for additional PQDs.

In addition to a blueshift in the PL spectra, a decrease in the size of the PQDs can also be inferred from the decreased absorption cross-section of single PQDs. In Figure 5a, the PL intensity of a single $CsPbI_3$ PQD declines slowly with time in dry nitrogen. During the decomposition process, we measure not only the spectral shift but also the PL intensity *I* and lifetime τ. The measured PL intensity *I* of a single QD is the product of the excitation rate η_{ex}, PL QY η, detection efficiency η_d, and the pulse repetition rate f as given by:

$$I = \eta_{ex} \times \eta \times \eta_d \times f, \qquad (1)$$

where $\eta = k_r\tau$, k_r is the radiative recombination rate, and τ is the PL lifetime. During the decomposition, the excitation rate η_{ex} decreases due to the shrinking volume of the PQD. The quantum yield η is also changing because of the change in the radiative recombination rate k_r and the non-radiative recombination rate k_{nr}. The excitation rate η_{ex} is proportional to the absorption cross-section σ at the excitation wavelength, 466nm. In the confocal system, the transmittances of the optical elements and quantum efficiency of the avalanche photodiodes remain flat from 680 nm to 590 nm. Therefore, the detection efficiency does not change for the blue-shifted fluorescence. Therefore, we can rewrite Equation (1) as

$$\frac{I}{\tau} \propto \sigma_{\lambda=466nm} \times k_r, \qquad (2)$$

which reflects the expected changes in the measured I/τ that occur as a consequence of photochemical changes in k_r and σ. As shown in Figure 5b, the slope of the fluorescence

lifetime and intensity distribution (FLID) becomes flatter after decomposition, implying a decrease in I/τ and thus in the product $\sigma_{\lambda=466nm} \times k_r$. The increased QD bandgap E_g and decreased I/τ are plotted every 10 s in Figure 5c. I/τ is also plotted as a function of E_g in Figure 5d.

In order to account for the observed trends in Figure 5d, we resort to a simple EMA model to estimate the evolution of the product of the absorption cross-section and the radiative recombination rate. For energy above the bandgap, $\sigma_{\lambda=466nm}$ is proportional to the volume of the QD, d^3; according to EMA, the difference between the bulk and QD bandgap energies, $E_g - E_g^{bulk}$, scales with the QD diameter as d^{-2}. Consequently, we have

$$\sigma_{\lambda=466nm} \propto \left(E_g - E_g^{bulk}\right)^{-1.5}, \qquad (3)$$

where $E_g^{bulk} = 1.73$ eV for bulk cubic $CsPbI_3$.[51]

It is difficult to determine the exact size dependence of the radiative recombination rate from experiment because we only measure the total recombination rate, which includes the contribution from non-radiative recombination.[52-55] From Fermi's golden rule, the transition rate k_{rmn} from the conduction state, $|c_m\rangle$, to the valence state, $|v_n\rangle$, in a homogeneous medium is given by:

$$k_{rmn} = \frac{ne^2}{3\pi\epsilon_0 m_0^2 \hbar c_0^3} \omega_{mn} |\langle c_m|P|v_n\rangle|^2, \qquad (4)$$

where n is the refractive index of the medium, e is the electron charge, ϵ_0 is the permittivity of the free space, m_0 is the electron mass, and the transition energy $\hbar\omega_{mn} = E_{cm} - E_{vn} +$

$E_g^{bulk} - E_b$. E_{cm} is the energy of the *m-th* subband of conduction, E_{vn} is the energy of *n-th* subband of the valence, and E_b is the binding energy of the exciton. The transition matrix element is given by the product of the electron and hole wavefunction overlap and the squared Bloch matrix element[52-53]

$$|\langle c_m|P|v_n\rangle|^2 = \sum_{i\ j} \left|\langle \phi_{mi}^c|\phi_{nj}^v\rangle\right|^2 \left|\langle u_i^c|P|u_j^v\rangle\right|^2, \quad (5)$$

where $u_i^c(r)$ and $u_j^v(r)$ are the *i-th* and *j-th* member of the orthogonal Bloch functions for the conduction and valence, respectively. The squared Bloch matrix element $\left|\langle u_i^c|P|u_j^v\rangle\right|^2$ does not depend on the size, however, both the order of sub-band energy levels and $\left|\langle \phi_{mi}^c|\phi_{nj}^v\rangle\right|^2$ do depend on the size. If we do not consider the complex band structure, then the transition matrix element is independent of size. In a two-level model where the conduction and valence band have only one Bloch function $u_0^c(r)$ and $u_0^v(r)$, Equation (5) becomes:

$$|\langle c_m|P|v_n\rangle|^2 = |\langle \phi_m^c|\phi_n^v\rangle|^2 |\langle u_0^c|P|u_0^v\rangle|^2. \quad (6)$$

This transition matrix element is size-independent.[52] In this way we have $k_r \propto E_g$.[52, 56-57] Then the relationship between I/τ and E_g is:

$$\frac{I}{\tau} \propto \sigma_{\lambda=466nm} \times k_r \propto E_g\left(E_g - E_g^{bulk}\right)^{-1.5}. \quad (7)$$

Although k_r increases slowly with E_g, $\sigma_{\lambda=466nm}$ decreases faster as $\left(E_g - E_g^{bulk}\right)^{-1.5}$ around 1.9-2.1 eV, resulting in the observed decrease in the values of $\sigma_{\lambda=466nm} \times k_r$ and I/τ. Equation (7) fits the experimental results for I/τ *vs* E_g in Figure 5d.

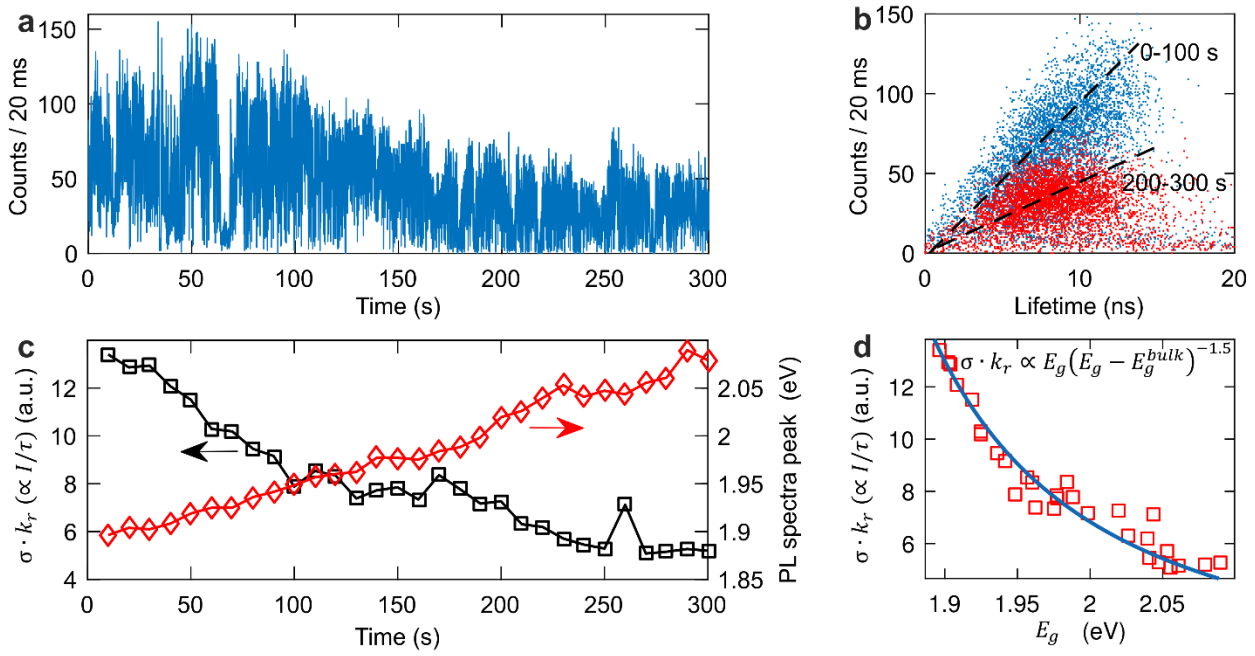

Figure 5 (a) PL intensity trajectory of a single $CsPbI_3$ PQD undergoing decomposition in dry nitrogen under a power of 100 nW (466 nm pulse laser, repetition rate 10 MHz). (b) Scatter plots of FLIDs for the first 100 s (blue dots) and the last 100 s (red dots). The dash lines indicate the FLID slopes. During the decomposition, the slope becomes flatter. (c) The product of absorption cross-section and radiative decay rate, $\sigma \cdot k_r$ ($\propto I/\tau$, black open squares), and the peaks of PL spectra (equal to the bandgap E_g, red open diamonds) as a function of time. (d) $\sigma \cdot k_r$ as a function of E_g (red open squares). The blue solid line is the fit using $E_g \cdot \left(E_g - E_g^{bulk}\right)^{-1.5}$, where E_g^{bulk} is equal to 1.73 eV.

In Table 1, we compare the intensity, lifetime, bandgap, radiative recombination rate, absorption cross-section and quantum yield for the initial and final emission states before and after the decomposition for 300 s. Although there is a 1.3-fold increase in the QY due to blinking or photo-chemical change, the absorption cross-section decreases more quickly,

thus leading to a decrease in the PL intensity. From the blueshift of the PL spectra together with I/τ , we can confirm that the decrease of QD size is due to decomposition.

Table 1 A comparison of final to initial emission state before and after decomposition in Figure 5

	I	τ	$k_r \propto E_g$	σ (a.u.)	$\eta \propto E_g \cdot \tau$ (a.u.)
Initial (10 s)	80 cts / 20ms	6.0 ns	1.896 eV	14.79	11.4
Final (300 s)	37 cts / 20ms	7.1 ns	2.079 eV	4.85	14.8
Ratio	0.46	1.18	1.10	0.33	1.30

For some stable $CsPbI_3$ PQDs, it is possible to examine the mechanism of blinking. Figure 6a shows second-order PL intensity correlation function, $g^2(t)$, measured for a single $CsPbI_3$ PQD in nitrogen under a 466 nm pulse laser (100 nW, 10 MHz, excitation rate $\eta_{ex} = 0.045$). The strong anti-bunching is a characteristic signature for single QD emission. The almost zero value of $g^2(t)$ at zero delay time implies highly efficient Auger recombination of the biexciton state. The PL intensity trajectory in Figure 6b contains sharp jumps between *on* and *off* states, which can be ascribed to the process of photoionization and neutralization.[37] The highly efficient Auger decay makes the emission intensity of trions much lower than that of neutral excitons, so it is difficult to extract the PL intensity and lifetime for trion emission from the PL intensity trajectory. In addition to the *on* and *off* states, in Figure 6b, there also exists a continuous distribution of grey states. The fluorescence lifetime and intensity distribution (FLID) in Figure 6c indicates a linear $I - \tau$ correlation for these

emission states. Since the single PQD did not degrade during the measurement, there should be no change in the absorption cross-section. Thus, the intensity is proportional to the radiative recombination rate and the PL lifetime:

$$I \propto \tau k_r. \qquad (8)$$

The linear FLID implies that the radiative recombination rate k_r is invariant for these grey states. This means that only the non-radiative recombination rate fluctuates among these grey and bright states. To further confirm this, we extract the lifetime from the PL decays for some emission states, showing that the PL intensity is a linear function of the lifetime (Figure S4 in Supporting Information). For three emission states with (I, τ), ((200 counts / 20 ms, 5.7 ns), (300 counts / 20 ms, 8.7 ns), and (400 counts / 20 ms, 10.4 ns)),we can compute the ratio of radiative recombination rates and we find it to be close to unity:

$$k_{r1}: k_{r2}: k_{r3} = \frac{I_1}{\tau_1}: \frac{I_2}{\tau_2}: \frac{I_3}{\tau_3} = 1: 0.98: 1.1 \ .$$

Blinking due to charge-discharge cycles also exists in these PQDs; however, the charged exciton state is almost non-emissive due to the fast Auger recombination. The radiative recombination rate of a trion is twice that of a neutral exciton,[58] so charging cannot be the reason for the linear correlation between lifetime and intensity. Similar blinking behaviors have been reported in CdSe/ZnS QDs,[59-60] which has been attributed to the activation and deactivation of non-radiative recombination centers.[61] Trap sites are proposed to be responsible for the blinking of giant organometallic perovskite crystals.[62-63] Shallow traps are

also found to exist in all-inorganic perovskite.[64] We postulate that the activation and deactivation of these traps modulate the non-radiative recombination rate and thus cause PL intensity jumps within a continuous distribution of emission states.

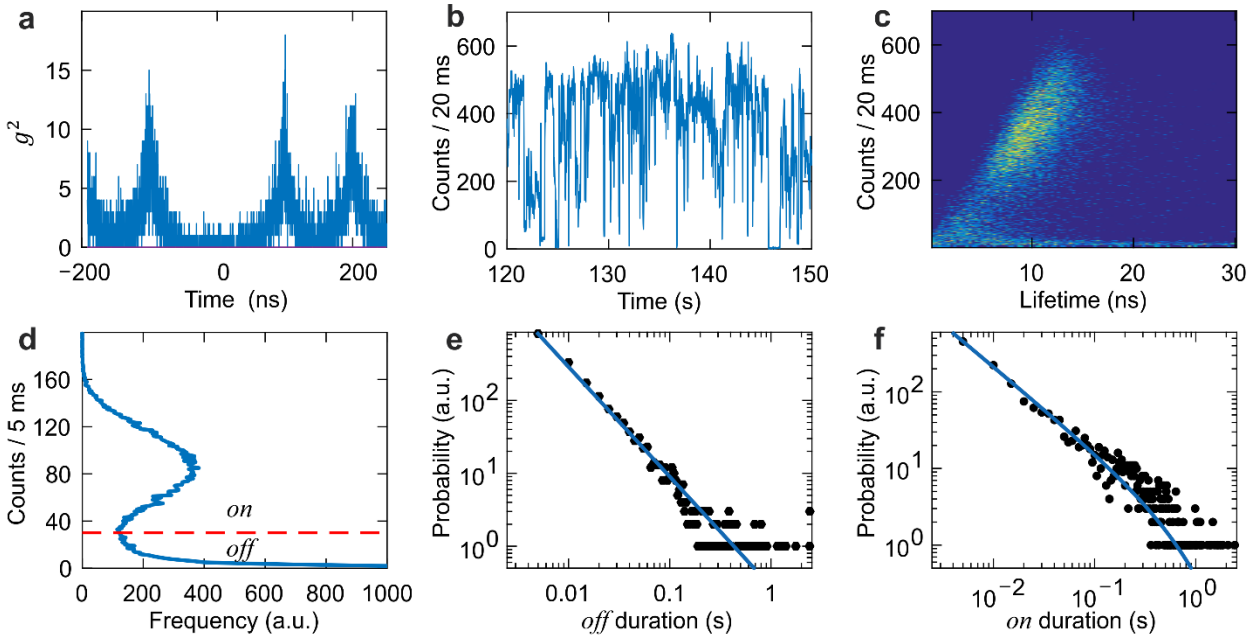

Figure 6 (a) Second-order PL intensity correlation function for a single $CsPbI_3$ PQD. The intensity at zero time is almost zero due to strong Auger quenching of biexcitons, indicating that it is really a single emitter. (b) PL intensity trajectory of the single PQD. A 20 ms bin is used. (c) FLID. There is a linear correlation between intensity and lifetime. (d) PL intensity histogram. A red dash line divides the emission into two parts: *on* and *off*. A 5 ms bin is used. Probability distributions of (e) *off* durations and (f) *on* durations are fitted to a power-law function and a truncated power-law function, respectively.

Despite the existence of continuous emission states due to the activation and deactivation of traps, we still use a threshold line in Figure 6d to differentiate *on* and *off* states from

charging and discharging cycles, for there are sharp changes in intensity between neutral and charged states. Instead of a 20 ms time bin used in Figures 6a-c, a 5 ms time bin is used to match the fast blinking in Figures 6d-f. Figure 6e gives the distribution of *off* durations which obeys a power-law function, $p_{off}(t) \propto t^{\alpha_{off}}$, where $\alpha_{off} = -1.51$. The distribution of *on* durations can be fitted to a truncated power-law function, $p_{on}(t) \propto t^{\alpha_{on}} exp(-t/\tau_c)$ with $\alpha_{on} = -1.1$ and $\tau_c = 0.768$ s. However, the truncated power law cannot describe the ionization process very well. A bi-exponential function fit is more exact as indicated by Figure S5 in Supporting Information. The power law can be explained as a sum of many exponential distributions; each of them is due to a trapping channel with a certain trapping time. When there are only two trapping channels, the power law reduces to a bi-exponential decay curve.

We address a final difference concerning the photodegradation of perovksite NCs in ensemble films and as single nanocrystals. In the case of perovskite nanocrystals in a film, a blue-shift was not apparent (Figure 1). However, in this case, we believe that only the uppermost layers of the nanocrystals are dissolving. The NCs underneath are protected and the fluorescence does not shift, because only a small fraction is blue-shifting and dissolving at any one time. Complete degradation takes some 10 hours in the case of the film due to the slow percolation of water vapour through the film. Hence it is the single nanocrystal data that provide better evidence for the mechanism of degradation.

CONCLUSIONS

In summary, we have investigated the degradation of single $CsPbI_3$ PQDs. By comparing the degradation rates in controlled humidity environments with gas and light, it is found that both light and water can independently degrade $CsPbI_3$. We also observed a blueshift in the emission spectra, which we attribute to gradual (layer-by-layer) decomposition of the PQDs. Furthermore, the absorption cross-section decreases and the radiative decay rate increases with the increase in optical bandgap. Single QD spectroscopy has identified two types of blinking mechanisms in the PQDs: one of them is consistent with the conventional charging and discharging process (*i.e.*, binary blinking), and the other involves the activation and deactivation of non-radiative recombination centers.

ASSOCIATED CONTENT

Supporting Information.

Figure S1: schematic of the chamber for measurement. Figure S2: absorption spectra, emission spectra, and a TEM image of $CsPbBr_3$ PQDs. Figure S3: continuous confocal scanning PL images of $CsPbBr_3$ PQDs. Figure S4: the correlation between the PL intensity and the PL lifetime. Figure S5: probability distribution of on durations is fitted to a bi-exponential function. The calculation of QD size based effective mass approximation (EMA) brief description is also available in Supporting Information.

AUTHOR INFORMATION

Corresponding Author

*E-mail: mulvaney@unimelb.edu.au

Notes

The authors declare no competing financial interests.

ACKNOWLEDGEMENTS

We acknowledge support from the ARC through the following grants: DP130102134 and CE170100026. G.Y. thanks the University of Melbourne for MIFR and MIEA scholarships. D.E.G. thanks the ARC for funding through a Future Fellowship (FT140100514).

REFERENCES

(1) Green, M. A.; Ho-Baillie, A.; Snaith, H. J. The Emergence of Perovskite Solar Cells. *Nature Photon.* **2014**, *8*, 506-514.

(2) Kojima, A.; Teshima, K.; Shirai, Y.; Miyasaka, T. Organometal Halide Perovskites as Visible-Light Sensitizers for Photovoltaic Cells. *J. Am. Chem. Soc.* **2009**, *131*, 6050-6051.

(3) Burschka, J.; Pellet, N.; Moon, S.-J.; Humphry-Baker, R.; Gao, P.; Nazeeruddin, M. K.; Gratzel, M. Sequential Deposition as a Route to High-Performance Perovskite-Sensitized Solar Cells. *Nature* **2013**, *499*, 316-319.

(4) Zhou, H.; Chen, Q.; Li, G.; Luo, S.; Song, T.-b.; Duan, H.-S.; Hong, Z.; You, J.; Liu, Y.; Yang, Y. Interface Engineering of Highly Efficient Perovskite Solar Cells. *Science* **2014**, *345*, 542-546.

(5) Jeon, N. J.; Noh, J. H.; Yang, W. S.; Kim, Y. C.; Ryu, S.; Seo, J.; Seok, S. I. Compositional Engineering of Perovskite Materials for High-Performance Solar Cells. *Nature* **2015**, *517*, 476-480.

(6) Protesescu, L.; Yakunin, S.; Bodnarchuk, M. I.; Krieg, F.; Caputo, R.; Hendon, C. H.; Yang, R. X.; Walsh, A.; Kovalenko, M. V. Nanocrystals of Cesium Lead Halide Perovskites ($CsPbX_3$, X = Cl, Br, and I): Novel Optoelectronic Materials Showing Bright Emission with Wide Color Gamut. *Nano Lett.* **2015**, *15*, 3692-3696.

(7) Akkerman, Q. A.; D'Innocenzo, V.; Accornero, S.; Scarpellini, A.; Petrozza, A.; Prato, M.; Manna, L. Tuning the Optical Properties of Cesium Lead Halide Perovskite Nanocrystals by Anion Exchange Reactions. *J. Am. Chem. Soc.* **2015**, *137*, 10276-10281.

(8) Nedelcu, G.; Protesescu, L.; Yakunin, S.; Bodnarchuk, M. I.; Grotevent, M. J.; Kovalenko, M. V. Fast Anion-Exchange in Highly Luminescent Nanocrystals of Cesium Lead Halide Perovskites ($CsPbX_3$, X = Cl, Br, I). *Nano Lett.* **2015**, *15*, 5635-5640.

(9) Bekenstein, Y.; Koscher, B. A.; Eaton, S. W.; Yang, P.; Alivisatos, A. P. Highly Luminescent Colloidal Nanoplates of Perovskite Cesium Lead Halide and Their Oriented Assemblies. *J. Am. Chem. Soc.* **2015**, *137*, 16008-16011.

(10) Li, J.; Xu, L.; Wang, T.; Song, J.; Chen, J.; Xue, J.; Dong, Y.; Cai, B.; Shan, Q.; Han, B., et al. 50-Fold Eqe Improvement up to 6.27% of Solution-Processed All-Inorganic Perovskite $CsPbBr_3$ QLEDs *via* Surface Ligand Density Control. *Adv. Mater.* **2017**, *29*, 1603885.

(11) Yantara, N.; Bhaumik, S.; Yan, F.; Sabba, D.; Dewi, H. A.; Mathews, N.; Boix, P. P.; Demir, H. V.; Mhaisalkar, S. Inorganic Halide Perovskites for Efficient Light-Emitting Diodes. *J. Phys. Chem. Lett.* **2015**, *6*, 4360-4364.

(12) Dai, X.; Deng, Y.; Peng, X.; Jin, Y. Quantum-Dot Light-Emitting Diodes for Large-Area Displays: Towards the Dawn of Commercialization. *Adv. Mater.* **2017**, *29*, 1607022.

(13) Zhang, L.; Yang, X.; Jiang, Q.; Wang, P.; Yin, Z.; Zhang, X.; Tan, H.; Yang, Y. M.; Wei, M.; Sutherland, B. R., et al. Ultra-Bright and Highly Efficient Inorganic Based Perovskite Light-Emitting Diodes. *Nat. Commum.* **2017**, *8*, 15640.

(14) Kulbak, M.; Cahen, D.; Hodes, G. How Important Is the Organic Part of Lead Halide Perovskite Photovoltaic Cells? Efficient $CsPbBr_3$ Cells. *J. Phys. Chem. Lett.* **2015**, *6*, 2452-2456.

(15) Swarnkar, A.; Marshall, A. R.; Sanehira, E. M.; Chernomordik, B. D.; Moore, D. T.; Christians, J. A.; Chakrabarti, T.; Luther, J. M. Quantum Dot–Induced Phase Stabilization of A-$CsPbI_3$ Perovskite for High-Efficiency Photovoltaics. *Science* **2016**, *354*, 92-95.

(16) Wang, Y.; Li, X.; Song, J.; Xiao, L.; Zeng, H.; Sun, H. All-Inorganic Colloidal Perovskite Quantum Dots: A New Class of Lasing Materials with Favorable Characteristics. *Adv. Mater.* **2015**, *27*, 7101-7108.

(17) Sutherland, B. R.; Sargent, E. H. Perovskite Photonic Sources. *Nature Photon.* **2016**, *10*, 295-302.

(18) Yakunin, S.; Protesescu, L.; Krieg, F.; Bodnarchuk, M. I.; Nedelcu, G.; Humer, M.; De Luca, G.; Fiebig, M.; Heiss, W.; Kovalenko, M. V. Low-Threshold Amplified Spontaneous Emission and Lasing from Colloidal Nanocrystals of Caesium Lead Halide Perovskites. *Nat. Commum.* **2015**, *6*, 8056.

(19) Yang, J.; Siempelkamp, B. D.; Liu, D.; Kelly, T. L. Investigation of $CH_3NH_3PbI_3$ Degradation Rates and Mechanisms in Controlled Humidity Environments Using *in Situ* Techniques. *ACS Nano* **2015**, *9*, 1955-1963.

(20) Leguy, A. M. A.; Hu, Y.; Campoy-Quiles, M.; Alonso, M. I.; Weber, O. J.; Azarhoosh, P.; van Schilfgaarde, M.; Weller, M. T.; Bein, T.; Nelson, J., et al. Reversible Hydration of $CH_3NH_3PbI_3$ in Films, Single Crystals, and Solar Cells. *Chem. Mater.* **2015**, *27*, 3397-3407.

(21) Eperon, G. E.; Habisreutinger, S. N.; Leijtens, T.; Bruijnaers, B. J.; van Franeker, J. J.; deQuilettes, D. W.; Pathak, S.; Sutton, R. J.; Grancini, G.; Ginger, D. S., et al. The Importance of Moisture in Hybrid Lead Halide Perovskite Thin Film Fabrication. *ACS Nano* **2015**, *9*, 9380-9393.

(22) Niu, G.; Li, W.; Meng, F.; Wang, L.; Dong, H.; Qiu, Y. Study on the Stability of $CH_3NH_3PbI_3$ Films and the Effect of Post-Modification by Aluminum Oxide in All-Solid-State Hybrid Solar Cells. *J. Mater. Chem. A* **2014**, *2*, 705-710.

(23) Conings, B.; Drijkoningen, J.; Gauquelin, N.; Babayigit, A.; D'Haen, J.; D'Olieslaeger, L.; Ethirajan, A.; Verbeeck, J.; Manca, J.; Mosconi, E., et al. Intrinsic Thermal Instability of Methylammonium Lead Trihalide Perovskite. *Adv. Energy Mater.* **2015**, *5*, 1500477.

(24) Yuan, X.; Hou, X.; Li, J.; Qu, C.; Zhang, W.; Zhao, J.; Li, H. Thermal Degradation of Luminescence in Inorganic Perovskite $CsPbBr_3$ Nanocrystals. *Phys. Chem. Chem. Phys.* **2017**, *19*, 8934-8940.

(25) Aristidou, N.; Sanchez-Molina, I.; Chotchuangchutchaval, T.; Brown, M.; Martinez, L.; Rath, T.; Haque, S. A. The Role of Oxygen in the Degradation of Methylammonium Lead Trihalide Perovskite Photoactive Layers. *Angew. Chem. Int. Ed. Engl.* **2015**, *54*, 8208-8212.

(26) Misra, R. K.; Aharon, S.; Li, B.; Mogilyansky, D.; Visoly-Fisher, I.; Etgar, L.; Katz, E. A. Temperature- and Component-Dependent Degradation of Perovskite Photovoltaic Materials under Concentrated Sunlight. *J. Phys. Chem. Lett.* **2015**, *6*, 326-330.

(27) Leijtens, T.; Eperon, G. E.; Pathak, S.; Abate, A.; Lee, M. M.; Snaith, H. J. Overcoming Ultraviolet Light Instability of Sensitized TiO_2 with Meso-Superstructured Organometal Tri-Halide Perovskite Solar Cells. *Nat. Commum.* **2013**, *4*, 2885.

(28) Li, Y.; Xu, X.; Wang, C.; Ecker, B.; Yang, J.; Huang, J.; Gao, Y. Light-Induced Degradation of $CH_3NH_3PbI_3$ Hybrid Perovskite Thin Film. *J. Phys. Chem. C* **2017**, *121*, 3904-3910.

(29) Chen, J.; Liu, D.; Al-Marri, M. J.; Nuuttila, L.; Lehtivuori, H.; Zheng, K. Photo-Stability of $CsPbBr_3$ Perovskite Quantum Dots for Optoelectronic Application. *Science China Materials* **2016**, *59*, 719-727.

(30) Pan, J.; Sarmah, S. P.; Murali, B.; Dursun, I.; Peng, W.; Parida, M. R.; Liu, J.; Sinatra, L.; Alyami, N.; Zhao, C., et al. Air-Stable Surface-Passivated Perovskite Quantum Dots for Ultra-Robust, Single- and Two-Photon-Induced Amplified Spontaneous Emission. *J. Phys. Chem. Lett.* **2015**, *6*, 5027-5033.

(31) Palazon, F.; Akkerman, Q. A.; Prato, M.; Manna, L. X-Ray Lithography on Perovskite Nanocrystals Films: From Patterning with Anion-Exchange Reactions to Enhanced Stability in Air and Water. *ACS Nano* **2016**, *10*, 1224-1230.

(32) Raja, S. N.; Bekenstein, Y.; Koc, M. A.; Fischer, S.; Zhang, D.; Lin, L.; Ritchie, R. O.; Yang, P.; Alivisatos, A. P. Encapsulation of Perovskite Nanocrystals into Macroscale Polymer Matrices: Enhanced Stability and Polarization. *ACS Appl. Mater. Interfaces* **2016**, *8*, 35523-35533.

(33) Wang, Y.; He, J.; Chen, H.; Chen, J.; Zhu, R.; Ma, P.; Towers, A.; Lin, Y.; Gesquiere, A. J.; Wu, S.-T., et al. Ultrastable, Highly Luminescent Organic–Inorganic Perovskite–Polymer Composite Films. *Adv. Mater.* **2016**, *28*, 10710-10717.

(34) Makarov, N. S.; Guo, S.; Isaienko, O.; Liu, W.; Robel, I.; Klimov, V. I. Spectral and Dynamical Properties of Single Excitons, Biexcitons, and Trions in Cesium-Lead-Halide Perovskite Quantum Dots. *Nano Lett.* **2016**, *16*, 2349-2362.

(35) Castaneda, J. A.; Nagamine, G.; Yassitepe, E.; Bonato, L. G.; Voznyy, O.; Hoogland, S.; Nogueira, A. F.; Sargent, E. H.; Cruz, C. H.; Padilha, L. A. Efficient Biexciton Interaction in Perovskite Quantum Dots under Weak and Strong Confinement. *ACS Nano* **2016**, *10*, 8603-8609.

(36) de Jong, E. M. L. D.; Yamashita, G.; Gomez, L.; Ashida, M.; Fujiwara, Y.; Gregorkiewicz, T. Multiexciton Lifetime in All-Inorganic $CsPbBr_3$ Perovskite Nanocrystals. *J. Phys. Chem. C* **2017**, *121*, 1941-1947.

(37) Park, Y. S.; Guo, S.; Makarov, N. S.; Klimov, V. I. Room Temperature Single-Photon Emission from Individual Perovskite Quantum Dots. *ACS Nano* **2015**, *9*, 10386-10393.

(38) Hu, F.; Zhang, H.; Sun, C.; Yin, C.; Lv, B.; Zhang, C.; Yu, W. W.; Wang, X.; Zhang, Y.; Xiao, M. Superior Optical Properties of Perovskite Nanocrystals as Single Photon Emitters. *ACS Nano* **2015**, *9*, 12410-12416.

(39) Aharonovich, I.; Englund, D.; Toth, M. Solid-State Single-Photon Emitters. *Nature Photon.* **2016**, *10*, 631-641.

(40) Raino, G.; Nedelcu, G.; Protesescu, L.; Bodnarchuk, M. I.; Kovalenko, M. V.; Mahrt, R. F.; Stoferle, T. Single Cesium Lead Halide Perovskite Nanocrystals at Low Temperature: Fast Single-Photon Emission, Reduced Blinking, and Exciton Fine Structure. *ACS Nano* **2016**, *10*, 2485-2490.

(41) Zhang, A.; Dong, C.; Ren, J. Tuning Blinking Behavior of Highly Luminescent Cesium Lead Halide Nanocrystals through Varying Halide Composition. *J. Phys. Chem. C* **2017**, *121*, 13314-13323.

(42) Hu, F.; Yin, C.; Zhang, H.; Sun, C.; Yu, W. W.; Zhang, C.; Wang, X.; Zhang, Y.; Xiao, M. Slow Auger Recombination of Charged Excitons in Nonblinking Perovskite Nanocrystals without Spectral Diffusion. *Nano Lett.* **2016**, *16*, 6425-6430.

(43) Seth, S.; Mondal, N.; Patra, S.; Samanta, A. Fluorescence Blinking and Photoactivation of All-Inorganic Perovskite Nanocrystals $CsPbBr_3$ and $CsPbBr_2I$. *J. Phys. Chem. Lett.* **2016**, *7*, 266-271.

(44) Swarnkar, A.; Chulliyil, R.; Ravi, V. K.; Irfanullah, M.; Chowdhury, A.; Nag, A. Colloidal $CsPbBr_3$ Perovskite Nanocrystals: Luminescence Beyond Traditional Quantum Dots. *Angew. Chem. Int. Ed. Engl.* **2015**, *54*, 15424-15428.

(45) Tachikawa, T.; Karimata, I.; Kobori, Y. Surface Charge Trapping in Organolead Halide Perovskites Explored by Single-Particle Photoluminescence Imaging. *J. Phys. Chem. Lett.* **2015**, *6*, 3195-3201.

(46) Pechstedt, K.; Whittle, T.; Baumberg, J.; Melvin, T. Photoluminescence of Colloidal CdSe/ZnS Quantum Dots: The Critical Effect of Water Molecules. *J. Phys. Chem. C* **2010**, *114*, 12069-12077.

(47) Müller, J.; Lupton, J. M.; Rogach, A. L.; Feldmann, J.; Talapin, D. V.; Weller, H. Air-Induced Fluorescence Bursts from Single Semiconductor Nanocrystals. *Appl. Phys. Lett.* **2004**, *85*, 381-383.

(48) Tice, D. B.; Frederick, M. T.; Chang, R. P. H.; Weiss, E. A. Electron Migration Limits the Rate of Photobrightening in Thin Films of CdSe Quantum Dots in a Dry N_2 (g) Atmosphere. *J. Phys. Chem. C* **2011**, *115*, 3654-3662.

(49) Carrillo-Carrion, C.; Cardenas, S.; Simonet, B. M.; Valcarcel, M. Quantum Dots Luminescence Enhancement Due to Illumination with Uv/Vis Light. *Chem. Commun.* **2009**, *0*, 5214-5226.

(50) Lorenzon, M.; Sortino, L.; Akkerman, Q.; Accornero, S.; Pedrini, J.; Prato, M.; Pinchetti, V.; Meinardi, F.; Manna, L.; Brovelli, S. Role of Nonradiative Defects and Environmental Oxygen on Exciton Recombination Processes in $CsPbBr_3$ Perovskite Nanocrystals. *Nano Lett.* **2017**, *17*, 3844-3853.

(51) Eperon, G. E.; Paternò, G. M.; Sutton, R. J.; Zampetti, A.; Haghighirad, A. A.; Cacialli, F.; Snaith, H. J. Inorganic Caesium Lead Iodide Perovskite Solar Cells. *J. Mater. Chem. A* **2015**, *3*, 19688-19695.

(52) van Driel, A. F.; Allan, G.; Delerue, C.; Lodahl, P.; Vos, W. L.; Vanmaekelbergh, D. Frequency-Dependent Spontaneous Emission Rate from CdSe and CdTe Nanocrystals: Influence of Dark States. *Phys. Rev. Lett.* **2005**, *95*, 236804.

(53) Stobbe, S.; Johansen, J.; Kristensen, P. T.; Hvam, J. M.; Lodahl, P. Frequency Dependence of the Radiative Decay Rate of Excitons in Self-Assembled Quantum Dots: Experiment and Theory. *Phys. Rev. B* **2009**, *80,* 155307.

(54) Gong, K.; Zeng, Y.; Kelley, D. F. Extinction Coefficients, Oscillator Strengths, and Radiative Lifetimes of CdSe, CdTe, and CdTe/CdSe Nanocrystals. *J. Phys. Chem. C* **2013**, *117*, 20268-20279.

(55) Angeloni, I.; Raja, W.; Polovitsyn, A.; De Donato, F.; Zaccaria, R. P.; Moreels, I. Band-Edge Oscillator Strength of Colloidal CdSe/CdS Dot-in-Rods: Comparison of Absorption and Time-Resolved Fluorescence Spectroscopy. *Nanoscale* **2017**, *9*, 4730-4738.

(56) Kayanuma, Y. Quantum-Size Effects of Interacting Electrons and Holes in Semiconductor Microcrystals with Spherical Shape. *Phys. Rev. B* **1988**, *38*, 9797-9805.

(57) Moreels, I.; Lambert, K.; Smeets, D.; De Muynck, D.; Nollet, T.; Martins, J. C.; Vanhaecke, F.; Vantomme, A.; Delerue, C.; Allan, G., et al. Size-Dependent Optical Properties of Colloidal PbS Quantum Dots. *ACS Nano* **2009**, *3*, 3023-3030.

(58) Jha, P. P.; Guyot-Sionnest, P. Trion Decay in Colloidal Quantum Dots. *ACS Nano* **2009**, *3*, 1011-1015.

(59) Zhang, K.; Chang, H.; Fu, A.; Alivisatos, A. P.; Yang, H. Continuous Distribution of Emission States from Single CdSe/ZnS Quantum Dots. *Nano Lett.* **2006**, *6*, 843-847.

(60) Schmidt, R.; Krasselt, C.; Göhler, C.; von Borczyskowski, C. The Fluorescence Intermittency for Quantum Dots Is Not Power-Law Distributed: A Luminescence Intensity Resolved Approach. *ACS Nano* **2014**, *8*, 3506-3521.

(61) Frantsuzov, P.; Volkán-Kacsó, S.; Jankó, B. Model of Fluorescence Intermittency of Single Colloidal Semiconductor Quantum Dots Using Multiple Recombination Centers. *Phys. Rev. Lett.* **2009**, *103*, 207402.

(62) Tian, Y.; Merdasa, A.; Peter, M.; Abdellah, M.; Zheng, K.; Ponseca, C. S., Jr.; Pullerits, T.; Yartsev, A.; Sundstrom, V.; Scheblykin, I. G. Giant Photoluminescence Blinking of Perovskite Nanocrystals Reveals Single-Trap Control of Luminescence. *Nano Lett.* **2015**, *15*, 1603-1608.

(63) Yuan, H.; Debroye, E.; Caliandro, G.; Janssen, K. P. F.; van Loon, J.; Kirschhock, C. E. A.; Martens, J. A.; Hofkens, J.; Roeffaers, M. B. J. Photoluminescence Blinking of Single-Crystal Methylammonium Lead Iodide Perovskite Nanorods Induced by Surface Traps. *ACS Omega* **2016**, *1*, 148-159.

(64) Mondal, N.; Samanta, A. Complete Ultrafast Charge Carrier Dynamics in Photo-Excited All-Inorganic Perovskite Nanocrystals ($CsPbX_3$). *Nanoscale* **2017**, *9*, 1878-1885.

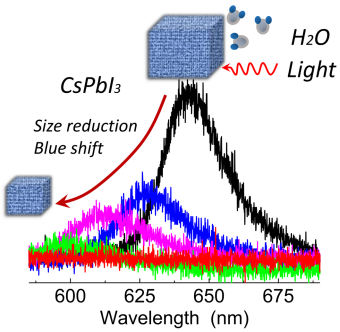
H2O
Light
CsPbI3
Size reduction
Blue shift
600
625
650
675
Wavelength (nm)